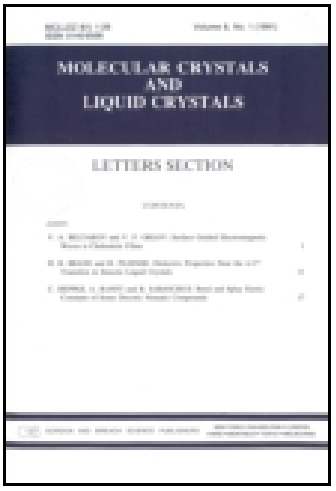

Molecular Crystals and Liquid Crystals
Publication details, including instructions for authors and subscription information:
http://www.tandfonline.com/loi/gmcl20

Electronic Processes and Energy Storage in Inorganic/Organic Nanohybrids

T. M. Bishchaniuk [a], O. V. Balaban [a], R. Ya. Shvets [a], I. I. Grygorchak [a], A. V. Fechan [a], B. A. Lukiyanets [a] & F. O. Ivashchyshyn [a]

[a] Lviv Polytechnic National University, 12, S. Bandery Str., Lviv, 79013, Ukraine

Published online: 28 Mar 2014.

To cite this article: T. M. Bishchaniuk, O. V. Balaban, R. Ya. Shvets, I. I. Grygorchak, A. V. Fechan, B. A. Lukiyanets & F. O. Ivashchyshyn (2014) Electronic Processes and Energy Storage in Inorganic/Organic Nanohybrids, Molecular Crystals and Liquid Crystals, 589:1, 132-140, DOI: 10.1080/15421406.2013.872404

To link to this article: http://dx.doi.org/10.1080/15421406.2013.872404

Mol. Cryst. Liq. Cryst., Vol. 589: pp. 132–140, 2014

ISSN: 1542-1406 print/1563-5287 online
DOI: 10.1080/15421406.2013.872404

Electronic Processes and Energy Storage in Inorganic/Organic Nanohybrids

T. M. BISHCHANIUK, O. V. BALABAN, R. YA. SHVETS, I. I. GRYGORCHAK,* A. V. FECHAN, B. A. LUKIYANETS, AND F. O. IVASHCHYSHYN

Lviv Polytechnic National University, 12, S. Bandery Str., Lviv 79013, Ukraine

Three types of nanohybridized structures such as organic/dielectric, organic/semiconductor, and organic/graphen-like ones are investigated. The effect of ultrasonic exposure on the material structure and its influence on the dielectric permeability and on the dielectric loss tangent are studied for the first type of nanostructures. The magnetoresistance of a structure at room temperature is studied in the second type of materials. The change of the kinetic parameters of the intercalation process is shown for the third type of nanohybrid structures.

Keywords Intercalation; impedance spectroscopy; dielectric loss tangent; ultrasonic irradiation; Gibbs' energy; graphen

Introduction

Recently, the formation of heterostructured inorganic/inorganic, inorganic/organic, and bio/inorganic nanocomposite materials attract the attention like a way of obtaining the structures with a wide range of new, unknown yet properties [1, 2]. However, the known methods of their production, such as vacuum deposition, photolithography, and synthetic Langmuir–Blodgett technique have certain reservations related to a limited variability in the choice of a variety of heteroingredients and the problematic synthesis of a "host-guest" architecture. Nonetheless, in the latest systems, one can achieve not only a directed change of the initial atomic-molecular structure and "hosts"-materials force fields, as well as the synthesis of chemical substances in a crystal field, but also to build certain structures on the atomic-molecular level and a whole functional blocks in the future. To carry out this, one can use the intercalation method of introduction of guest components into the crystal structure in areas of the action of van der Waals' forces of the host materials. The intercalation technologies are intended to create the set of complicated atomic-molecular complexes. Intercalation methods have a certain sequence of chemical reactions and, at the same time, provide a reliable anticoagulation matrix isolation of nanosystems [3].

The progress achieved in this way, cannot be considered as impressive yet. Currently, only a limited experience is accumulated, and just the first steps are done [4–6]. Therefore, the aim of this paper is an attempt to fill the gap in this research area.

*Corresponding author, I. I. Grygorchak. Tel.: +38(032) 258-27-08. E-mail: ivan_gryg@ukr.net

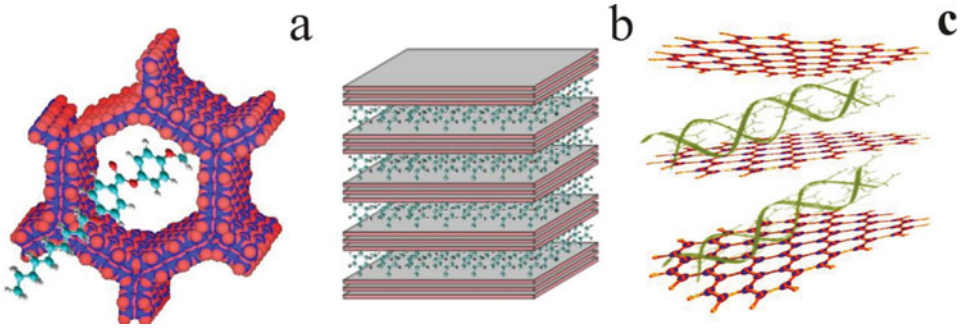

Figure 1. The schematic representation of organic/dielectric (a) organic/semiconductor (b) and organic/graphen like nanohybridized structures fragments (c).

Methodology of Experiment

According to the three main groups of zonal structures, the organic/nonconductor, the organic/semi-conductor, and the organic/graphen-like nanohybrids were formed, and they are schematically represented in Fig. 1.

For the first type of nanostructures, the "host" material was a mesoporous molecular-lattice regular structure on the basis of SiO_2. In the scientific literature, this nanostructure is known as MCM-41 [7]. It has a hexagonal honeycomb-like structure with wall thickness within 0.6–0.8 nm and calibrated pore size. According to the electron microscopy data, the pore size is about 37 Å. The guest content was a ferroelectric liquid crystal (LC), which consists of the *C* achiral smectic (a phenylbenzoate derivative) and a chiral component. Its implementation in MCM-41 was achieved by using the known method that is described in [8, 9], for example. According to it, the samples to study were formed at the same time. The samples were like a tablet 5 mm in diameter and 1.4 mm in thickness. One can see the schematic representation of MCM-41 with encapsulated LC structure (MCM-41<LC>) in Fig. 1a.

The gallium selenide (GaSe) and indium selenide (InSe) layered semiconductors were used as a semiconductor matrix for the second type of nanohybrids. Single crystals grown by the Bridgman–Stockbarger method had a clearly pronounced layered structure and, respectively, the *p*- and *n*-types of conductivity. The bandgap (according to the optical data) was 2.02 eV for the first type of single crystals and 1.22 eV for the second type. As is well known [10, 11], they are characterized by the presence of the so-called "guest" positions that are oriented perpendicularly to the crystallographic *C*-axis of the areas with weak van der Waals' forces. The introduction of foreign ions, atoms, or molecules into the interior crystal spaces is known as the intercalation phenomenon [12]. As far as the LC molecules or other macromolecules are introduced directly neither in GaSe nor in InSe, so the three-stage "crystalengineering" scheme was used to form intercalated nanostructures. At the first stage, sodium nitrite is introduced in the original matrix by the direct exposure method in its melt of a single semiconductor crystal at a temperature of 300°C during 5–10 min. As a result of the *n*-stage ordering [13, 14], the distance between the layers significantly increases. The next step was the deintercalation of sodium nitrite from the crystal by its extraction during the 24-h fivefold cycle and drying at a temperature of 110°C and a reduced pressure. Deintercalated, weakened by the van der Waals bonds, and modified by interior force fields in a crystal, InSe and GaSe matrices became suitable to the introduction of LC macromolecules. Therefore, at the third stage, the ferroelectric liquid crystal or other

organic content was encapsulated in the extended crystal lattice by the direct exposure at room temperature during 48 h in its saturated solution or melt. The thickness of GaSe samples was 0.15 mm. After the intercalation, the thickness of a GaSe<LC> structure increases by several times (0.65 mm), the squared area being 4.7×2.8 mm^2. One can see the schematic representation of the obtained structure in Fig. 1b.

To form a nanohybrid of the third type, we made initially the expansion of a graphite crystal lattice by the microwave (a frequency of 2458 MHz) irradiation of the I stage separation hydrolyzed intercalated graphite during one minute. On the first stage, the structure of a nanohybrid was multilayered and consisted of graphen (G) sheets and gaps between them. The mechanism of expansion of the graphite crystal lattice during the microwave irradiation was the following. At the first step, the small amount of graphite was placed in a microwave oven. The material under study contains structural water. When the own oscillation frequency of water molecules is equal to the microwave frequency, the phenomenon of resonance occurs. As a result, water molecules move. At the same time, one can see the process of expansion of the whole material. The next encapsulation of an organic "guest" was based on the above-mentioned methods [8, 9]. The "guests" were thiourea ($CS(NH_2)_2$) and L-aspartic acid (LAA). The prepared encapsulated materials (G<$CS(NH_2)_2$> and G<LAA>) are ready to be studied. The active mass of electrodes was 3 mg.

Impedance measurements in the direction of the crystallographic C-axis were performed in the frequency range 10^{-3}–10^6 Hz with a measuring complex "AUTOLAB" (firm "ECO CHEMIE," Netherlands) equipped with computer programs FRA-2 and GPES. The frequency dependence of the complex impedance Z was analyzed by the graphical-analytical method in the software package ZView 2.3 (Scribner Associates). Approximation errors were less than 4%. Thermodynamic regularities of the Li^+–intercalation current formation were investigated in a three-electrode cell with one molar solution $LiBF_4$ in γ-butyrolactone with a chlorine-silver reference electrode.

Results and Discussion

Having a low electronic conductivity (conditioned by own defects), the MCM-41 mesoporous matrix and MCM-41<LC> nanohybrid may be of interest, especially for Dielectronics.

As far as structures' quality is an important parameter, we will consider the conditions, under which the dielectric loss tangent is less than 1. Figure 2 shows that there are two frequency ranges, in which this requirement is ensured, and the fundamental ability to control this parameter by ultrasonic irradiation. The frequency range from 0.3 Hz to 1 Hz is an area of intensive relaxation processes, in which the dielectric loss tangent reaches the maximum values of 4–6 for all three structures. The corresponding behavior of the permittivity (ε) is shown in Fig. 3.

The observed combination of a high value of ε with a low value of tg δ is essential for the formation of high-capacity radiofrequency capacitors. It should be noted that ultrasonic irradiation provides such combination also for infra-low frequencies. This investigation may open a new approach to the creation of quantum batteries as a modern alternative to chemical current sources. The former are the systems, in which the accumulation and storage of an energy are realized not through electrochemical processes, but by the accumulation and storage of light electrons at interfaces within nanostructured systems.

The second-type nanohybrids can be widely used in the semiconductor technique and, in particular, due to their high photosensitivity, in Nanophotoelectronics. Figure 4 shows

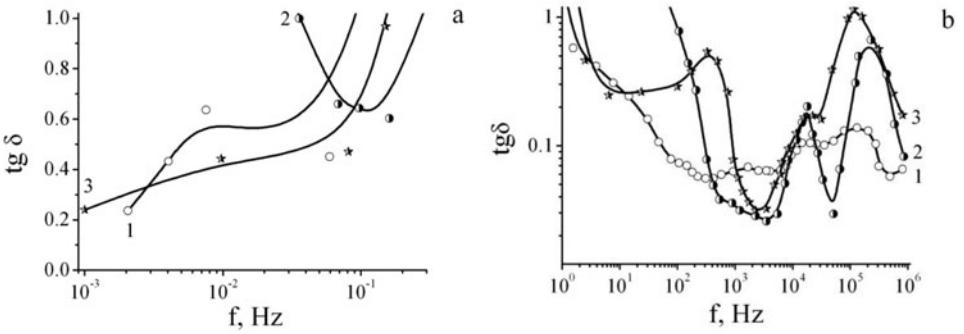

Figure 2. Frequency dependences of the dielectric loss tangent of the initial matrix MCM-41 (1), MCM-41 <LC> nanohybrid before (2) and after (3) ultrasonic irradiation at infra-low frequencies (a) and in the range of $1–10^6$ Hz (b).

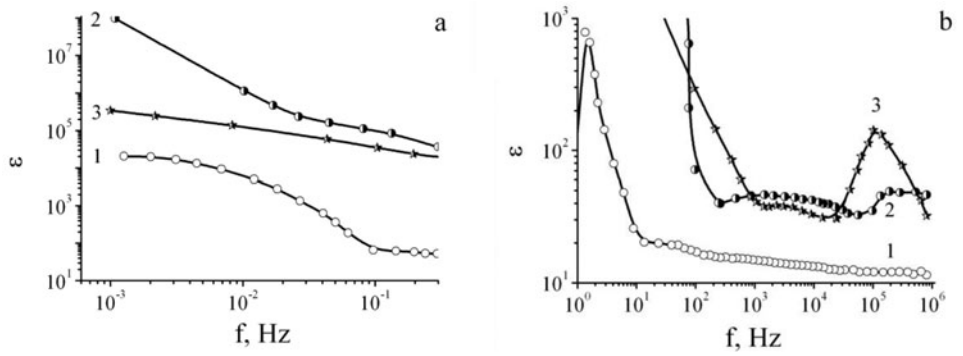

Figure 3. Frequency dependences of the dielectric constant of the initial matrix MCM-41 (1), MCM-41<LC> nanohybrid before (2) and after (3) ultrasonic irradiation at infra-low frequencies (a) and in the range of $1–10^6$ Hz (b).

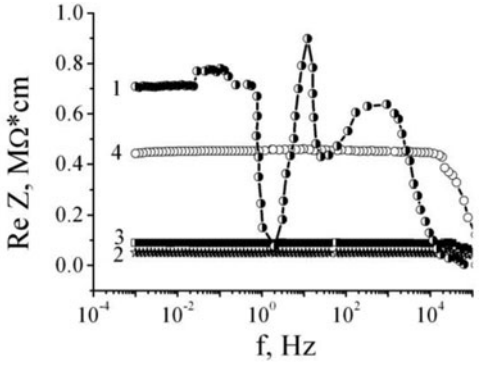

Figure 4. The frequency dependences of the real part of the specific impedance perpendicular to the layers of extended matrix of GaSe with encapsulated LC, measured at 293 K in the dark (1), in light (2) and at imposing a constant magnetic field along the crystallographic *C*-axis (3). (4) - extended crystalline matrix.

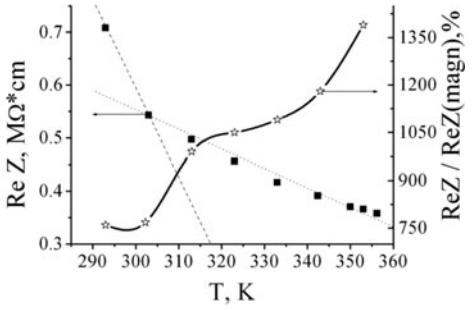

Figure 5. Temperature dependence of the real part of the impedance and the magnetoresistance of GaSe<LC> along the crystallographic *C*-axis.

the frequency dependences of the real part of the complex specific impedance that is perpendicular to the planes of GaSe<LC> nanolayers under different conditions of the experiment. It is seen that, at room temperature (293 K) without external fields, Re *Z* for the output extended matrix of GaSe behaves itself in the usual way: the low-frequency branch becomes descending at high frequencies due to the contribution of the hopping conductivity through localized states near the Fermi level, or due to the processes of excitation by capturing them in tails of the zone or in the zone of delocalized states [15, 16]. The encapsulation of LC causes an unusual behavior of Re *Z* (f), because a strong deformation of the low-frequency branches arises, which indicates the appearance of the inductive response of nanohybrid structures [17]. These deformations disappear under the illumination by visible light or in a magnetic field imposed along the crystallographic *C*-axis, as shown in Fig. 4. However, the resistance is reduced by 1.5 orders of magnitude in the first case and almost by 8 times in the second one, showing a huge magnetoresistance of the photosensitive structure at room temperature in a weak magnetic field. This phenomenon can find its application to Spintronics. The mechanism of the observed giant negative magnetoresistance is likely associated with the Zeeman delocalization of charge carriers with a simultaneous reduction of the ratio of the densities of states above and below the Fermi level in its δ - vicinity. Not only the magnetic field, but also the thermal delocalization can be promoted for such nature. Indeed, as is shown in Figs. 5 and 6, the conductance and the negative magnetoresistance grow with the temperature.

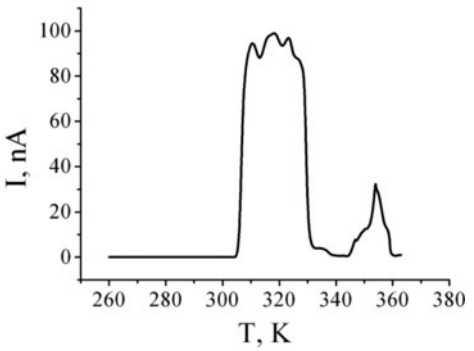

Figure 6. Temperature dependence of the current of thermally stimulated depolarisation of GaSe<LC> along the crystallographic *C*-axis.

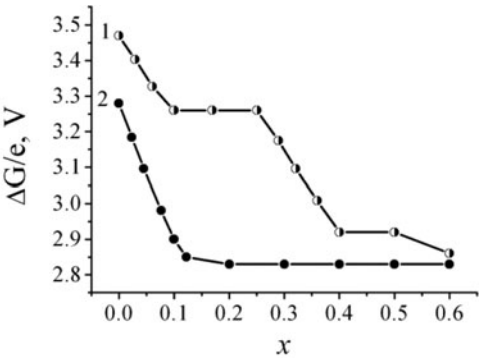

Figure 7. The Gibbs' energy change of the lithium intercalation process G<$CS(NH_2)_2$<Li_x>> at 33% - (1) and 100% - (2) filling intergraphene gaps by supramolecular kavitand.

However, the energy relief of such nanohybrid provides an opportunity to form internal electric fields under certain conditions. Indeed, the spectrum of thermostimulated depolarization researches showed the appearance of the thermogalvanic effect, as shown in Fig. 6. It is worth noting that its appearance is correlated with the energy change of the activation conductivity (Fig. 5). It is obvious that this effect can be useful for the development of new methods of direct conversion of thermal energy into electrical energy and the creation of a nanothermogenerator of electricity.

Organic/graphen-like nanohybrids have the highest electrical conductivity compared to the previous two types of synthesized nanostructures. Forming them into a hierarchical architecture <"subhost" <"host" for lithium>>, in which an intermediate host is a supramolecular cavitand, can lead not only to entirely new patterns of interphase charge transfer, but also to the highly effective Faraday energy accumulation. The thermodynamic rationale for this approach is based on the entropy and enthalpy stabilization of the Gibbs' free energy change $\Delta G(x)$ of the intercalation reaction as a function of the implemented guest component concentration in accordance with the equation [18]

$$\Delta G(x) = eE = \mu_i(x) - \mu_0 = kT \ln \left| \frac{x}{1-x} \right| + N\omega x + [E_F(x) - E_F(0)] + \frac{\partial C}{L \partial x} + E_0, \quad (1)$$

where x is the number of "guest" embedded atoms of the component, which are related to one basic structural unit of the "host" material; $\mu_i(x)$ is the chemical potential of the embedded "guest" component in the "host" matrix; μ_0 is a chemical potential in a metal anode; k is the Boltzmann constant; N is the number of the nearest neighboring seats; ω is the energy of interaction of embedded "guest" components; E_F is the position of the Fermi level; C is the crystal lattice parameter; L is a coeficient; and E_0 is the "guest-host" interaction energy. The drop reduce of $\Delta G(x)$, as x increases, can be achieved by a directional control of the second and third terms of Eq. (1) by controlled changes of the own energy spectrum and the impurity one. This would allow one to "design" the desired kind of a discharge curve (of course, with the exception of the initial and final stages of the discharge [19]). Actually, the placement of the "host-guest" system in the force crystalline field of a "subhost", which forms a fractalization intercalation complex, is a possible effective method of achieving this goal. At the same time, the use of an intermediate host supramolecular cavitand will allow one to create a huge amount of supramolecular structures with quite paradoxical properties.

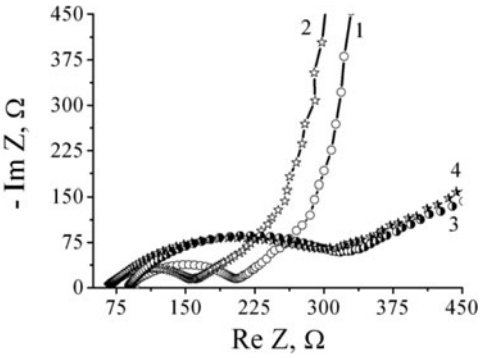

Figure 8. Nyquist diagrams of the lithium intercalation process G<CS(NH$_2$)$_2$<Li$_x$>> at 33% and 100% filling of intergraphene gaps by supramolecular kavitand respectively for $x = 0$ (1) and (2) and $x = 0.5$ - (3) and (4).

Figure 7 shows the Gibbs' energy change in the Li^+–intercalation current creation reactions in G<CS(NH$_2$)$_2$<Li$_x$>> with various contents of thiourea.

One can see that the degree of filling of the intergraphen gaps (υ) by the supramolecular cavitand affects the value of $\Delta G(x)$ and, in addition, changes its character as a function of x, i.e., the phase characteristics at the implementation of lithium compounds G<CS(NH$_2$)$_2$<Li$_x$>>. It turns out that υ noticeably changes the kinetic parameters of the process. Thus, Figure 8 shows that, at the initial stages of the lithium intercalation, the increaseg of the filling degree of intergraphene gaps by a supramolecular cavitand reduces the resistance to the charge transfer from the electrolyte into the supramolecular structure, which increases, in turn, the current creation power.

It is revealed that, for the of Li^+–intercalation current creation, we can successfully use the other organic content (LAA) between extended graphene layers. It is one of the twenty standard aminoacids that are found as a part of proteins of all living organisms. At the isoelectric point (the value of pH at which the total charge of the aminoacid molecule is equal to zero), aminoacids are zwitter ions that have properties of an anion and a cation. Zwitter ions are neutral molecules containing parts that carry positive and negative charges which

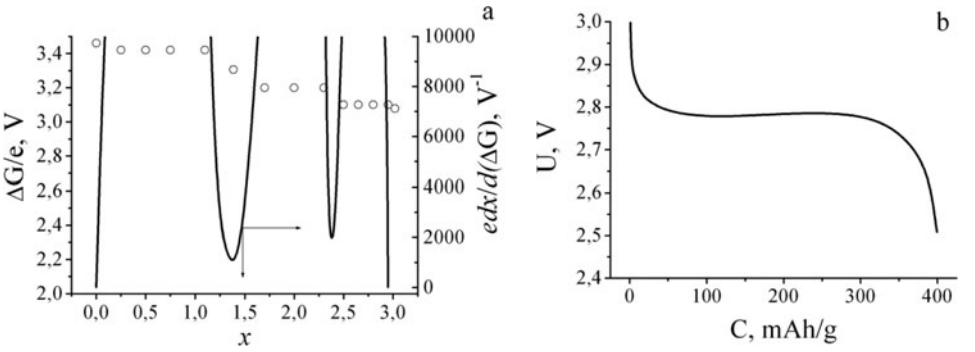

Figure 9. The change of Gibbs' energy of the lithium intercalation process G<CS(NH$_2$)$_2$<Li$_x$>> - (circles) and differential capacitance-(solid line) as functions of the degree of the guest load (a). The discharge curve at the current loading of 3 mA/g (b).

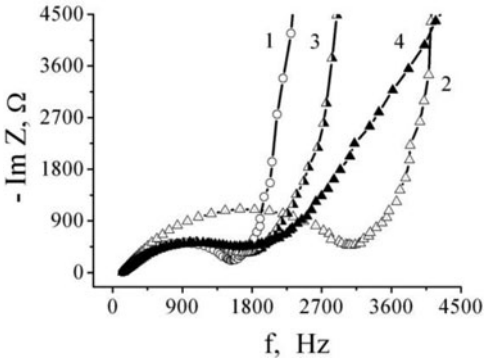

Figure 10. Nyquist diagrams for G<LAA<Li_x>>: 1 - for $x = 0$; 2 - for x at 1st phase transition of first kind; and 3 - for x at 2nd phase transition of first kind, 4 - for x at 3rd phase transition of first kind.

are localized at different atoms. As a result, such a molecule has a huge dipole moment and can be a receptor of cations and anions as well. Figure 9 shows a change of Gibbs' energy of the lithium intercalation process as a function of the galvanostatic discharge duration for the supramolecular ensemble with the hierarchical architecture G<LAA>. On the concentration axis characterizing the guest load, we can see three intervals of independence of Gibbs' free energy change of the Li^+ implementation reaction ($0.25 < x < 1$, $1.7 < x < 2.3$, $2.5 < x < 3$), for which the derivatives $\partial x/\partial(\Delta G)$ are sent to infinity, indicating the first-order phase transition, namely, the existence of biphase areas in these intervals that alternate with single-phase states. The last ones correspond to the formation of a row of nonstoichiometric intercalation compounds G<$CS(NH_2)_2$<Li_x>>: corresponding chronopotentiograms for every measured value of x represent parallels to the time axis shifted to the negative region relative to the chlorine-silver electrode in proportion to the amount of missed electricity [20]. The regions of the points of minimum at $x \sim 1.35$ and 2.37 are most often associated with the guest subsystem ordering [21].

The Nyquist diagrams (Fig. 10) show that the charge transfer resistance is a nonmonotonic function of the lithium guest load degree. For the initial stage of implementation, as well as for values of x from the first and second intervals of phase transitions of the first kind, the slope of the low-frequency branch to the axis of the real part of the impedance on the Nyquist diagrams is different from 45°, indicating that the limiting diffusion in the structure does not obey Fick's law. Only as the concentration of embedded lithium increases with transition to the third region, the diffusion becomes close to the ideal one and can be modeled by the equivalent Rendels–Erschler scheme [22].

Conclusions

The dielectric loss tangent of the MCM-41<LC> structure possesses the value less than 1 with simultaneous huge increase in the permittivity within two frequency regions (at infra-low frequencies and at $1–10^6$ Hz), which makes it attractive for Dielectronics.

The ultrasonic exposure of the MCM-41<LC> structure provides a combination of the ultrahigh ε value with low dielectric loss tangent at the infra-low frequency region, which makes the development of quantum accumulators possible.

There is the tremendous eightfold decrease in the magnetoresistance at room temperature in the GaSe<LC> structure that can be used in Spintronics. This phenomenon can be associated with the Zeeman delocalization of charge carriers with a simultaneous decrease in the ratio of the densities of states below and under the Fermi level at its neighborhood of δ.

The occupancy of grafen interfaces by the supramolecular cavitand affects the $\Delta G(x)$ value and the kinetic parameters of the intercalation of $G<CS(NH_2)_2<Li_x>>$, which leads to an increase in the current forming power.

The character of Gibbs' energy change under the lithium intercalation in the supramolecular ensemble with the hierarchical architecture G<LAA> indicates the presence of a first-kind phase transition. The limiting diffusion does not obey Fick's law at the first stages of intercalation, but returns to the ideal diffusion in the third region.

References

[1] Choy, J. H., Kwon, S. J., & Park, G. S. (1998). *Science*, *280*, 1589.

[2] Choy, J. H., Kwak, S. Y., Park, J. S., Jeong, Y. J., & Portier, J. (1999). *Am. Chem. Soc.*, *121*, 1399.

[3] Gusev, A. I. (1998). *Usp. Fiz. Nauk.*, *168*, 55.

[4] Grygorchak, I. I., Seredyuk, B. O., Tovstyuk, K. D., & Bakhmatyuk, B. P. (2002). In: *New Trends in Intercalation Compounds for Energy Storage*, Dordrecht: Kluwer, 543.

[5] Voitovych, S. A., Grygorchak, I. I., & Aksimentyeva, O. I. (2008). *Mol. Cryst. Liq. Cryst.*, *497*, 55.

[6] Jin-Ho Choy, Seung-Min Peak, Jae-Min Oh, & Eue-Soon Jang. (2002). *Curr. Appl. Phys.*, *2*, 489.

[7] Peter, C. T. (2004). *Amer. Chem. Soc.*, *26*, 2879.

[8] Voinov, Yu. P., Gabitova, N. F., Gorkelik, V. S., & Sverbil', P. P. (2009). *Solid State Physics*, *51*(7), 1333.

[9] Baryshnikov, S. V., Charnaya, E. V., Milinskyy, A.Yu., Stukova, E. V., Cheng, Tien, Bohlmann, W., & Michel, D. (2010). *Solid State Physics*, *51*(6), 1172.

[10] Kuhn, A., Chevy, A., & Chevalier, R. (1975). *Phys. Status Sol.*, *A31*, 469.

[11] Chevy, A., Kuhn, A., & Martin, M. S. (1977). *J. Cryst. Growth.*, *38* (1), 118.

[12] Friend, R. H., & Yoffe, A. D. (1987). *Adv. Phys.*, *36*(1), 1.

[13] Safran, S. A. (1987). *Solid State Physics: Adv. Res. and Appl.*, *40*, 246.

[14] Grigorchak, I. I., Netyaga, V. V., Kovalyuk, Z. D. (1997). *J. Phys.: Condens. Mater.*, *9*, L191.

[15] Pollak, M., & Geballe, T. H. (1961). *Phys. Rev.*, *122*, 1742.

[16] Olekhnovich, N. M., Moroz, I. I., Pushkarev, A. V., Radyush, Yu.V., & Salak, A. N. (2008). *Phys. Solid State*, *50*(3), 472.

[17] Pokladok, N. T., Grygorchak, I. I., Grygorchak, O. I., Ivashchyshyn, F. O., & Stahira, P. I. (2010). *Sensor Electronics and Microsystem Technologies, 7*(4), 69.

[18] Nagelberg, S., & Worrell, W. L. (1981). *J. Solid State Chemistry*, *38*, 321.

[19] McKinnon, W. R., & Haering, R. R. (1983). *Modern Aspects of Electrochemistry*, *15*, 235.

[20] Kabanov, B. N., Chekavtsev, A. V., Petukhova, P. I., Tomashova, N. N., & Kiselyov, I. G. (1986). *Electrochemistry*, *22*(3), 415.

[21] Thompson, A. G. (1980). *Phys. B + C*, *99B*(1–4), 100.

[22] Stoynov, Z. B., Grafov, B. M., Savova–Stoynova, B., & Elkin V. V. (1991). *Electrochemical Impedance*, Moscow: Nauka (in Russian).